Electronic Supplementary Material (ESI) for Physical Chemistry Chemical Physics.

Electronic Supplementary Information (ESI)

Electron and excitation energy transfers in covalently linked donor-acceptor dyads: mechanisms and dynamics revealed by quantum chemistry

Lorenzo Cupellini*[a], Samuele Giannini[a,b], Benedetta Mennucci*[a]

---

[a] *Dipartimento di Chimica e Chimica Industriale, University of Pisa, Via Moruzzi 3, 56124 Pisa, Italy. E-mail: Benedetta.Mennucci@unipi.it lorenzo.cupellini@for.unipi.it*

[b] *Current affiliation: Department of Physics and Astronomy, University College London, Gower Street, London WC1E 6BT, UK*

S1 Structure and fragment definition

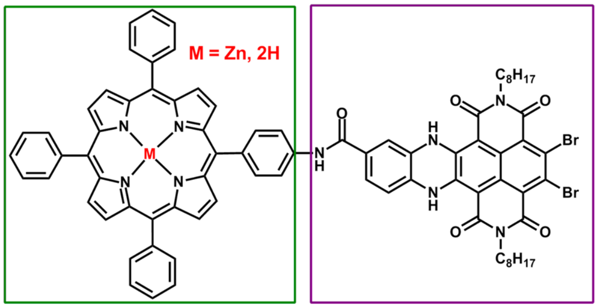

Fig. S1 Structure of the porphyrin-naphthalenediimide dyads. The colored boxes show the definition of molecular fragments as used in all calculations. The green box surrounds the ZnP and FbP fragments, whereas the purple ones surround the HNDI fragment.

S2 Analysis of Natural Transition Orbitals

In this section we report the Natural Transition Orbitals (NTOs) for selected transitions of ZnP-HNDI (Figure S2) and FbP-HNDI (Figure S3), as well as the transitions of their constituents in Figures S4, S5, and S6.

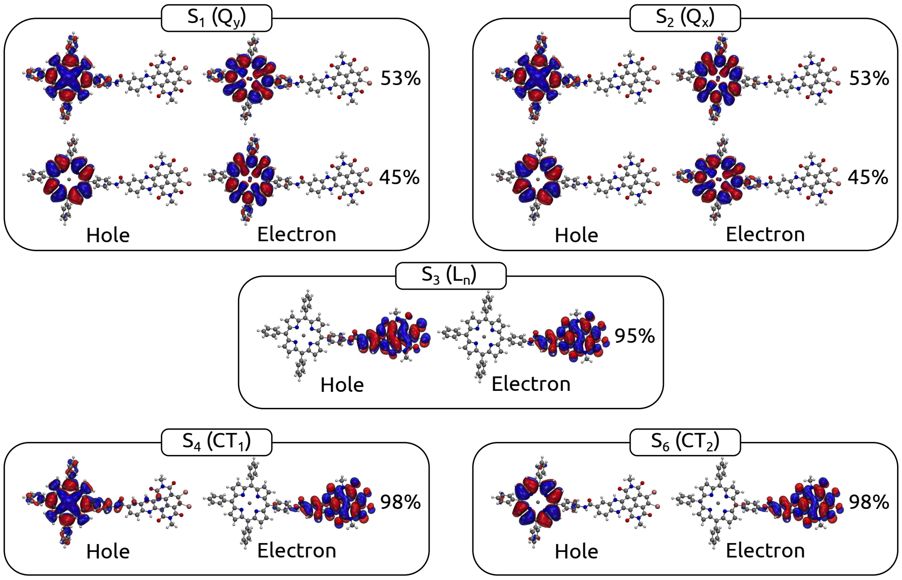

Fig. S2 Natural Transition Orbitals for the main excited states of ZnP-HNDI.

The transitions localized on ZnP or FbP follow the symmetry derived by the four-orbital model proposed by Martin Gouterman.[1,2] Within such model the orbitals involved in the electronic transitions are a pair of frontier molecular orbitals (*i.e.* HOMO and LUMO). Their mixing explains the presence of two pairs of degenerate states with e_u symmetry in ZnP. The degeneracy is removed in FbP due to the broken symmetry. In both porphyrins, the low-energy Q_x and Q_y states carry a small oscillator strength, whereas the two other high energy bands (Soret bands) have large oscillator strengths. As seen in Figures S5 and S6, both Q transitions are described by the same pairs of NTOs.

The Q states in both (Figure S3) and ZnP-HNDI (Figure S2) are mainly localized on the porphyrin macrocycle, although both hole and electron NTOs show some delocalization over the meso-phenyl substituents. The L_n state is $\pi \rightarrow \pi^*$ state delocalized over the whole HNDI moiety, and also on the amide bond that links the two moieties. The two CT states of ZnP-HNDI correspond to the movement of an electron from the two ZnP HOMO to the HNDI LUMO. In fact, the hole NTOs of the CT states are identical to the two hole NTOs of the Q states, and for both CT states the electron NTO corresponds to the π^* electron NTO of the L_n state.

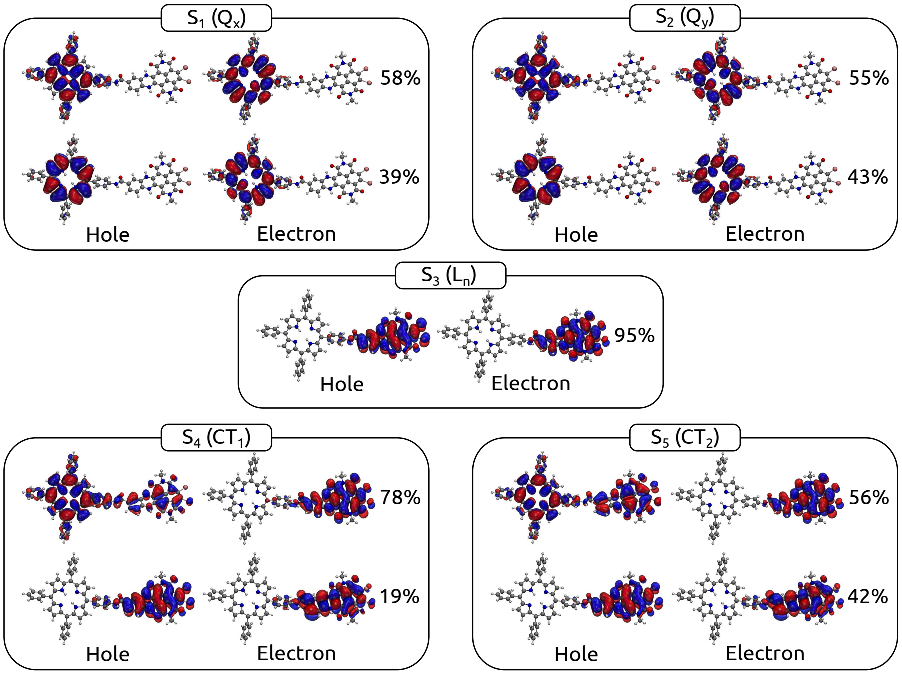

Fig. S3 Natural Transition Orbitals for the main excited states of FbP-HNDI.

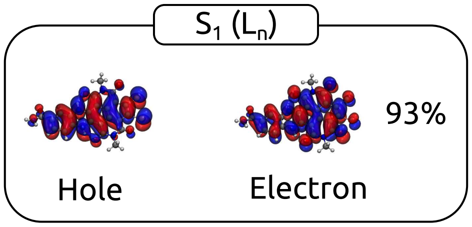

Fig. S4 Natural Transition Orbitals for the L$_n$ state of HNDI.

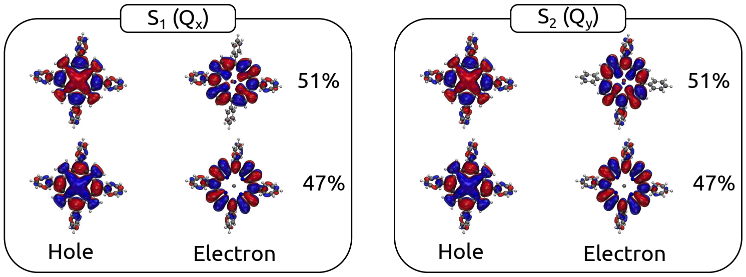

Fig. S5 Natural Transition Orbitals for the Q excited states of ZnP.

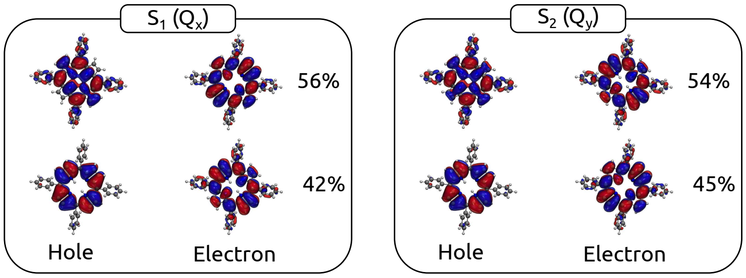

Fig. S6 Natural Transition Orbitals for the Q excited states of FbP.

S3 Excitation energies and functional dependence

In the following we report excitation energies for ZnP-HNDI and FbP-HNDI obtained with TD-DFT and TDA-DFT and different functionals. These data have been used to benchmark the vertical energies of both dyads. The excitation energies and oscillator strengths are very similar both in THF (Table S1 and toluene (Table S2) .

Table S1 Excitation energies (eV) of porphyrin-HNDI dyads and isolated fragments, calculated with TDA-CAM-B3LYP/6-311+G(d,p) in THF.[a]

State	Dyad		Fragments			Exp.[b]
	ZnP-HNDI	FbP-HNDI	ZnP	FbP	HNDI	
Qx	2.37 (0.023)	2.22 (0.022)	2.37 (0.008)	2.22 (0.016)	—	2.30
Qy	2.37 (0.006)	2.40 (0.038)	2.37 (0.006)	2.40 (0.018)	—	2.30
Ln	2.59 (1.407)	2.59 (1.400)	—	—	2.60 (1.103)	2.23
CT1	3.36 (0.068)	3.41 (0.249)	—	—	—	
CT2	3.55 (0.073)	3.70 (0.013)	—	—	—	

[a] The calculated oscillator strengths are reported in brackets. [b] The approximate experimental vertical energies are referred to the ZnP and HNDI systems.

Table S2 Excitation energies (eV) of porphyrin-HNDI dyads and isolated fragments, calculated with TDA-CAM-B3LYP/6-311+G(d,p) in Toluene.[a]

state	Dyad		Fragments		
	ZnP-HNDI	FbP-HNDI	ZnP	FbP	HNDI
Qx	2.37 (0.017)	2.21 (0.017)	2.38 (0.005)	2.21 (0.013)	-
Qy	2.38 (0.004)	2.40 (0.039)	2.38 (0.004)	2.40 (0.020)	-
Ln	2.59 (1.386)	2.59 (1.384)	-	-	2.60 (1.102)
CT1	3.28 (0.030)	3.28 (0.031)	-	-	-
CT2	3.44 (0.010)	3.55 (0.227)	-	-	-

[a] The calculated oscillator strengths are reported in brackets (A.U.).

We can observe in Table S3 that transition energies may vary using different functionals, however the dipole moments result less variable especially for localized transitions. Two exceptions are the B3LYP functional in ZnP-HNDI and the PBE0 in FbP-HNDI. In those cases the dipole moments are quite different from the other results as the states are much more mixed. In particular, the L_n mixes with the Q states and its dipole moments decreases. Since the dipole moment is quite robust with different functionals and we are interested in an accurate description of the transition densities, rather than in the vertical energies, we can conclude that these functionals give a reliable description of the former quantities.

Table S3 Excitation energies (eV) of porphyrin-HNDI dyads calculated with various functionals and TDA-DFT/6-311+G(d,p) in THF.[a]

		CAM-B3LYP	M06-2X	PBE0	B3LYP
ZnP-HNDI	Qx	2.37 (0.4)	2.42 (0.6)	2.35 (3.1)	2.30 (10.0)
	Qy	2.37 (0.1)	2.42 (0.1)	2.35 (0.2)	2.31 (0.3)
	Ln	2.59 (22.2)	2.59 (22.6)	2.40 (20.5)	2.33 (14.2)
	CT1	3.36 (0.8)	3.15 (0.1)	2.07 (1.0)	2.92 (0.7)
	CT2	3.55 (0.8)	3.37 (0.0)	2.30 (0.0)	2.94 (0.0)
FbP-HNDI	Qx	2.22 (0.4)	2.27 (0.5)	2.22 (0.7)	2.17 (1.0)
	Qy	2.40 (0.7)	2.46 (1.0)	2.37 (7.7)	2.34 (3.1)
	Ln	2.59 (22.1)	2.59 (22.5)	2.40 (15.8)	2.32 (20.9)
	CT1	3.41 (3.0)	3.22 (0.2)	2.13 (1.3)	1.91 (0.8)
	CT2	3.70 (0.1)	3.40 (3.2)	2.45 (0.1)	2.23 (0.1)

[a] Squared dipole moments for these transitions are reported in brackets (A.U.).

As can be seen in Table S4, TD-DFT includes the de-excitations mechanism and gives smaller transitions energy compared with TDA-DFT, however even this method does not produce the correct energy ordering for these systems.[3]

Table S4 Excitation energies (eV) of ZnP-HNDI calculated with TDDFT-CAM-B3LYP/6-311+G(d,p) and TDA-CAM-B3LYP/6-311+G(d,p) in Vacuo

	CAM-B3LYP		M06-2X	
	TDDFT	TDA	TDDFT	TDA
Qx	2.24	2.39	2.31	2.44
Qy	2.24	2.39	2.31	2.44
Ln	2.55	2.75	2.55	2.75
CT1	3.22	3.22	3.00	3.01
CT2	3.34	3.34	3.15	3.15

Table S5 Excitation energies (eV) of ZnP-HNDI calculated with TDDFT-CAM-B3LYP/6-311+G(d,p) and TDDFT-M062X/6-311+G(d,p) in THF and Toluene

	THF		Toluene	
	CAMB3LYP	M06-2X	CAMB3LYP	M06-2X
Qx	2.22	2.29	2.22	2.30
Qy	2.22	2.29	2.22	2.30
Ln	2.41	2.42	2.42	2.42
CT1	3.37	3.14	3.29	3.07
CT2	3.56	3.37	3.44	3.25

S4 Basis sets dependence

Different basis sets have been tested for calculating the EET, ET, HT and CR coupling values. As for EET couplings also in for charge transfer calculations the largest basis set was used.

Table S6 Calculated EET couplings (cm^{-1}) for ZnP-HNDI obtained with FED and DC approaches.

	FED			DC		
	Vacuo	THF	Toluene	Vacuo	THF	Toluene
6-31G(d)	75.5	66.3	56.7	44.0	37.2	30.8
6-31+G(d)	75.5	66.6	56.8	48.1	36.8	30.4
6-311+G(d,p)	70.9	63.1	53.5	45.0	34.3	28.1

Table S7 Calculated ET, HT and CR couplings (cm^{-1}) for ZnP-HNDI obtained including 2 states in the FCD procedure

	Electron Transfer			Hole Transfer			Charge recombination		
	Vacuo	THF	Toluene	Vacuo	THF	Toluene	Vacuo	THF	Toluene
6-31G(d)	83.0	94.8	88.1	208.1	253.3	231.5	270.9	476.5	368.3
6-31+G(d)	89.9	105.0	96.6	223.7	266.9	243.9	293.3	513.1	398.0
6-311+G(d,p)	88.3	103.1	94.5	236.2	272.6	247.9	300.4	549.2	412.6

S5 Benchmark of FCD couplings

Test calculations were carried out to investigate the EET, ET, HT and CR couplings obtained by using the fragment difference approaches. In Table S7, FED and FCD couplings are calculated employing different basis and solvents (in the former case 2 states are included in diabatization state, whereas in the latter we used 10). The results are really similar for both functionals, but for the CR couplings that shows larger differences. The reasons is due to the coupling convergence that is not yet reached with 10 states for such mechanisms. The electronic states involved in CT processes can be well separated in energy from each other, therefore the lowest adiabatic states are likely the combination of several CT and locally excited states. This condition leads to inaccurate coupling values when only two states are used for the diabatization.[4–6] For this reason, we employed the multi-state FCD framework to compute charge-transfer couplings.[5] In Figure S7 we report the dependence on the number of states in the multi-state FCD procedure for the three different transfer processes in THF as a solvent.

Table S8 Calculated coupling (cm^{-1}) obtained using CAMB3LYP and M062X in different solvent with the 6-311+G(d,p) basis set.[a]

		ZnP-HNDI		FbP-HNDI	
		CAMB3LYP	M062x	CAMB3LYP	M062x
Vacuo	EET	70.9	78.9	50.7	-
THF	EET	63.1	70.4	45.7	50.7
	ET	102.7	109.2	86.35	86.8
	HT	268.0	264.0	243.36	257.4
	CR	360.4	328.0	236.87	287.5
Toluene	EET	53.5	59.9	38.6	-
	ET	94.7	100.6	80.6	-
	HT	247.2	245.5	240.4	-
	CR	325.7	301.6	304.0	-

[a] The FCD method for ET, HT, CR includes only 10 states (after this number of states the M062x functional shows convergence problems)

Although ET and HT couplings present a low dependence from the number of states included in the diabatization space, the CR coupling shows an irregular downwards behaviour, reaching a stable plateau only when more than 22 states are included in the multi-state FCD. For such reason, every calculation regarding charge transfer processes is performed by using 24 excited states in the diabatization procedures.

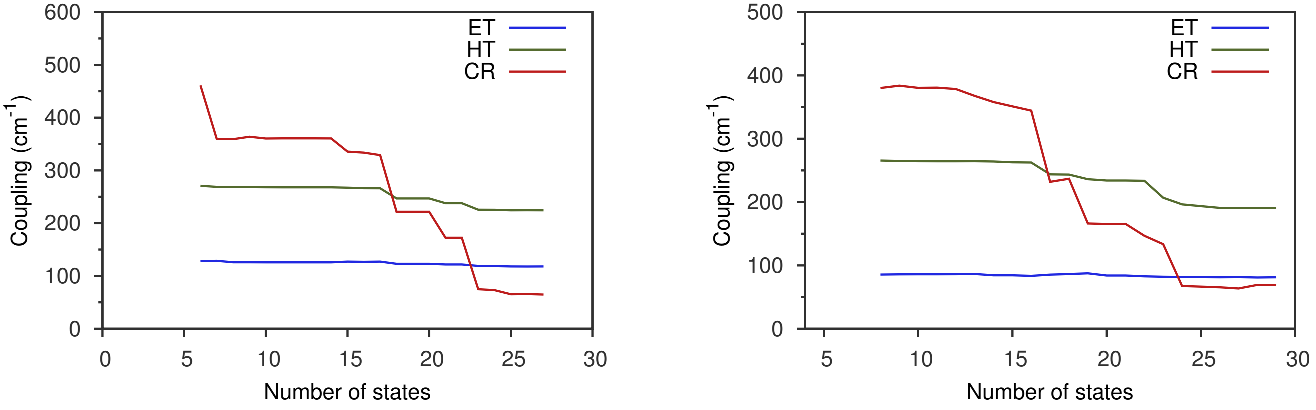

(a) **(b)**

Fig. S7 FCD couplings (cm^{-1}) for (a) ZnP-HNDI and (b) FbP-HNDI as a function of the number of excited states included in the diabatization procedure. The solvent is THF.

S6 Calculation of charge transfer driving force

In order to assess the quality of the redox calculations, we compared our calculated oxidation (for ZnP/FbP) and reduction (for HNDI) potentials with the experimental data available in literature. To the best of our knowledge, for such systems, electrochemical measures are accessible only in dichloromethane (DCM), thus we performed calculations in DCM to compare with redox experiments. In literature the oxidation and reduction potentials are often referred to different electrodes, therefore, after a careful conversion between electrodes, we have reported in Table S9 the absolute value of such experimental potentials directly comparable with our data.

Unfortunately, there is no experimental data available for the reduction potential of the HNDI molecule used in the present work, even though very similar molecules have been systematically studied.[7] For such reason we were forced to rely on a chemical analogue of our HNDI molecule. In particular, we utilized the reduction potential of molecule 2b present in the Supporting Information of Ref. 8. Its value is -1.24 eV and is referred to the ferrocene electrode in DCM solvent. We calculated the reduction potential of this HNDI analogue using the same solvent to assess the validity of our calculations (see Table S9).

Table S9 Redox potentials for ZnP, FbP, and HNDI in different solvents, and calculated ΔG for charge separation and recombination.[a]

		THF	toluene	DCM	DCM (Exp.)[a]
ZnP-HNDI	E_{ox}	5.308	5.663	5.279 (-1.2%)	5.344
	E_{red}	3.449	3.084	3.617[b] (-1.3%)	3.664[b]
	$E_{ox} - E_{red}$	1.86	2.579	-	-
	ΔG_B	-0.106	-0.345	-	-
FbP-HNDI	E_{ox}	5.373	5.655	5.344 (-4.6%)	5.604
	E_{red}	3.449	3.084	3.617[b] (-1.3%)	3.664[b]
	$E_{ox} - E_{red}$	1.924	2.571	-	-
	ΔG_B	-0.106	-0.345	-	-

[a] The oxidation potential of ZnP and FbP in DCM are 0.82 and 1.08 eV respectively and they refer to the SCE electrode.[9,10] The benchmark value for the SHE electrode, used to retrieve the absolute redox potential from experimental values, is 4.28 eV and it was obtained using *ab intio* high-quality calculations.[11]

[b] these data refer to the HNDI analogue found in Ref. 8

It is worth noting that, for the ZnP-HNDI, the errors obtained for oxidation and reduction potentials are very similar and have the same sign, so we expect an error cancellation when computing ΔG. On the contraty, for FbP-HNDI, the oxidation potential of the donor is a bit underestimated, which would underestimate also the difference. We can argue that, despite some dissimilarities with the experimental values, overall our calculations are in reasonable agreement with the experimental values in DCM. Assuming that the method error remains the same for different solvents, we can use the redox potentials in THF and toluene to calculate charge separation and recombination Gibbs free energies (see Table 2 in the main text) and rates (see Table 3 in the main text). Finally, we can observe that the binding energy is the same for the two systems as the structural differences are negligible.

S7 Spectral fitting

In order to extract the effective mode frequency for the Marcus-Levich-Jortner equation, we fitted the absorption spectrum $A(E)$ of HNDI with a single-mode expression:

$$A(E) = \sum_m \left(1 - \frac{m\hbar\omega}{E_0}\right)^3 \frac{S_{\mathrm{exc}}^m}{m!} \exp\left(\frac{(E - E_0 + m\hbar\omega)^2}{2\sigma^2}\right) \tag{S1}$$

The fit parameters E_0 and ω correspond to the 0-0 transition energy and to the vibrational frequency, S_{exc} is the Huang-Ryhs factor associated with the excitation, and σ is the broadening of each vibronic band. Note that S_{exc} is not the Huang-Ryhs factor used in eq. (6), as the latter is associated with the transfer of an electron.

S8 Details on the kinetic model

Once the kinetic constants characterizing the different steps of the excited state dynamics have been found, we can build a kinetic scheme able to couple various processes. Here we report the coupled differential equations for ZnP-HNDI (Eq. S2) and FbP-HNDI (Eq. S3) respectively:

$$\begin{cases} \frac{\mathrm{d}P_Q}{\mathrm{d}t} = -(k_{Q\to L_n} + k_{Q\to CSS})P_Q + k_{L_n\to Q}P_{L_n} \\ \frac{\mathrm{d}P_{L_n}}{\mathrm{d}t} = -(k_{L_n\to Q} + k_{L_n\to CSS})dP_{L_n} + k_{Q\to L_n}P_Q \\ \frac{\mathrm{d}P_{CSS}}{\mathrm{d}t} = k_{L_n\to CSS}P_{L_n} + k_{Q\to CSS}P_Q \\ \frac{\mathrm{d}P_{GS}}{\mathrm{d}t} = k_{CSS\to GS}P_{CSS} \end{cases} \tag{S2}$$

$$\begin{cases} \frac{\mathrm{d}P_{Q_x}}{\mathrm{d}t} = -(k_{Q_x\to L_n} + k_{Q_x\to CSS} + k_{Q_x\to T})P_{Q_x} + k_{L_n\to Q_x}P_{L_n} \\ \frac{\mathrm{d}P_{L_n}}{\mathrm{d}t} = -(k_{L_n\to Q_x} + k_{L_n\to CSS})dP_{L_n} + k_{Q_x\to L_n}P_{Q_x} \\ \frac{\mathrm{d}P_{CSS}}{\mathrm{d}t} = k_{L_n\to CSS}P_{L_n} + k_{Q_x\to CSS}P_{Q_x} \\ \frac{\mathrm{d}P_{GS}}{\mathrm{d}t} = k_{CSS\to GS}P_{CSS} \\ \frac{\mathrm{d}P_T}{\mathrm{d}t} = k_{Q_x\to T}P_{Q_x} \end{cases} \tag{S3}$$

where we follow the notation of eq. 11 in the main text. Each of these two systems can be rewritten using a matricial form as:

$$\frac{\mathrm{d}\mathbf{P}(t)}{\mathrm{d}t} = \mathbf{K}\mathbf{P}(t) \tag{S4}$$

in which $\mathbf{P}(t)$ is a column vector containing population of different states and $\mathbf{K}$ is a square matrix composed by the transfer rate constants. Eq. (S4) can be solved imposing initial condition for $\mathbf{P}(0)$ and writing:

$$\mathbf{P}(t) = e^{\mathbf{K}t}\mathbf{P}(0) \tag{S5}$$

diagonalizing $\mathbf{K}$ as:

$$\mathbf{K}\mathbf{X} = \mathbf{X}\Lambda \tag{S6}$$

and inserting eq. (S6) in eq. (S5) we find:

$$\mathbf{P}(t) = \mathbf{X}e^{\Lambda t}\mathbf{X}^{-1}\mathbf{P}(0) \tag{S7}$$

the effective rate constants correspond to the elements of the diagonal Λ matrix.

References

1 M. Gouterman, *J. Chem. Phys.*, 1959, **30**, 1139.
2 M. Gouterman, 1963, **127**, 108–127.
3 A. Dreuw and M. Head-Gordon, *Chem. Rev.*, 2005, **105**, 4009–37.
4 Z.-Q. You and C.-P. Hsu, *Int. J. Quantum Chem.*, 2014, **114**, 102–115.
5 C.-H. Yang and C.-P. Hsu, *J. Chem. Phys.*, 2013, **139**, 154104.
6 A. A. Voityuk, *J. Phys. Chem. C*, 2013, **117**, 2670–2675.
7 N. Sakai, J. Mareda, E. Vauthey and S. Matile, *Chem. Commun.*, 2010, **46**, 4225–4237.
8 A. L. Sisson, N. Sakai, N. Banerji, A. Fürstenberg, E. Vauthey and S. Matile, *Angew. Chemie Int. Ed.*, 2008, **47**, 3727–3729.
9 N. Banerji, S. V. Bhosale, I. Petkova, S. J. Langford and E. Vauthey, *Phys. Chem. Chem. Phys.*, 2011, **13**, 1019–1029.
10 A. Giraudeau, H. J. Callot and M. Gross, *Inorg. Chem.*, 1979, **18**, 201–206.
11 A. A. Isse and A. Gennaro, *J. Phys. Chem. B*, 2010, **114**, 7894–7899.